



4th International Conference on Silicon Photovoltaics, SiliconPV 2014

## Mercury: A back junction back contact front floating emitter cell with novel design for high efficiency and simplified processing

Ilkay Cesar\*, Nicolas Guillevin, Antonius R. Burgers, Agnes A. Mewe, Martien Koppes, John Anker, L.J. Geerligs, Arthur W. Weeber

*ECN Solar Energy, P.O. Box 1, 1755 ZG Petten, The Netherlands*

---

### Abstract

The back junction back contact cell, and more specifically the interdigitated back contact (IBC) cell is among the most appropriate cell designs to achieve highly efficient solar cells. An important aspect to improve manufacturability (e.g. reduce cost) of the cell and module is to increase the rear side back surface field (BSF) region width, as this currently constitutes the smallest feature size in the diffusion pattern of the IBC cell. We propose a novel design of an IBC cell that enhances the effective lateral transport of minority carriers (holes) and therefore allowing wide BSF regions. The novel design feature is to implement an appropriate conductive and well passivated  $p^{++}$ -doped layer, referred to as a front floating emitter (FFE), on the front surface of the IBC cell. This conductive FFE enables equally-sized interdigitated doping patterns of positive and negative polarities on the rear, with similar cell pitch and efficiency compared to traditional IBC cells. It also enables larger interconnection pads for easier module interconnection with marginal loss of cell performance. Additional advantages are expected from relaxed alignment tolerances as well as interconnection. We report on the proof-of-principle of this new cell concept, which we name “Mercury”, brought forward by 2D simulations and experimental results on small and 6 inch cells, based on an industrial process flow with stable results. So far, these cells yield efficiencies up to 19.4% and short-circuit densities well above 41 mA/cm<sup>2</sup>. Additionally, the Mercury cells show less efficiency loss at low illumination intensity than a standard p-type H-pattern cell.

© 2014 The Authors. Published by Elsevier Ltd. This is an open access article under the CC BY-NC-ND license (<http://creativecommons.org/licenses/by-nc-nd/3.0/>).

Peer-review under responsibility of the scientific committee of the SiliconPV 2014 conference

*Keywords:* Front floating emitter, IBC, silicon, solar cell, electrical shading, back surface field.

---

---

\* Corresponding author. Tel.: +31-(0)224-564217; fax: +31-(0)224-568214.  
*E-mail address:* [cesar@ecn.nl](mailto:cesar@ecn.nl)

## 1. Introduction

IBC cells are an ideal candidate for high-efficiency solar cells mainly because all metallization can be placed on the rear side of the cell which reduces shading losses. The industrial manufacturability of these cells has been demonstrated by Sunpower for many years. Recently, the company reported on the industrial production of 5 inch IBC cells with median efficiencies as high as 24.1% [1]. Recent achievements by others are worth mentioning. A consortium of ANU and Trina have reported on a  $2 \times 2 \text{ cm}^2$  IBC cell with a top efficiency of 24.6% featuring local back surface field (BSF) diffusions at the contacts and an undiffused front side that is passivated by a dielectric stack [2]. IMEC obtained on  $2 \times 2 \text{ cm}^2$  23.1% [3]. A process based on implanted surface diffusions is reported by Bosch Solar achieving 22.1% on  $239 \text{ cm}^2$  cells [4]. Also, Samsung together with Varian reported on IBC cells prepared by implantation on  $155 \text{ cm}^2$  with 22.4% efficiency [5]. The high performance of these cells is partially obtained because of contact technologies such as PVD in combination with electroplating. These contacts exhibit much lower contact recombination losses than the conventional screen-print technology based on fire-through silver pastes. However, ISC Konstanz has reported on 6 inch IBC cells with screen-printed contacts with up to 21.3% efficiency, illustrating the potential of that low-cost approach [6]. Also Hareon presented on screen printed IBC solar cell and achieved 19.6% in 6 inch Cz [7].

Although interdigitated back contact (IBC) solar cells have shown to yield very high conversion efficiencies, cost-effective production of these devices poses challenges. To allow all contacts to be placed on the rear of the cell, the rear collecting junction, the emitter, is interrupted by a non-collecting junction, the BSF. Any carrier that is photo-generated above a BSF area, needs to travel laterally to an emitter area. If the BSF regions become too wide, the collection probability of carriers generated above the BSF will decrease: an effect referred to as electrical shading [8]. To prevent loss in cell performance, the typical width of the BSF is in the order of 0.4 mm out of a typical cell pitch of 1.5 mm.

The inequality of widths of BSF and emitter results in strict patterning tolerances for processing but has also implications for the metallization. As equal current needs to flow through both emitter and BSF contacts towards the interconnection points, which are located mostly at the edge of the cell, a dilemma can be identified for the PVD or plated contacts in combination with unequal diffusion widths. Either a metal volume redundancy, with corresponding high cost, of the emitter contact is accepted, or an insulating layer has to be inserted between the BSF contact electrodes and cell to allow equal metal cross-sections for emitter and BSF without shunts from BSF contact to emitter surface. These two design options are illustrated in Figure 1a and 1b.

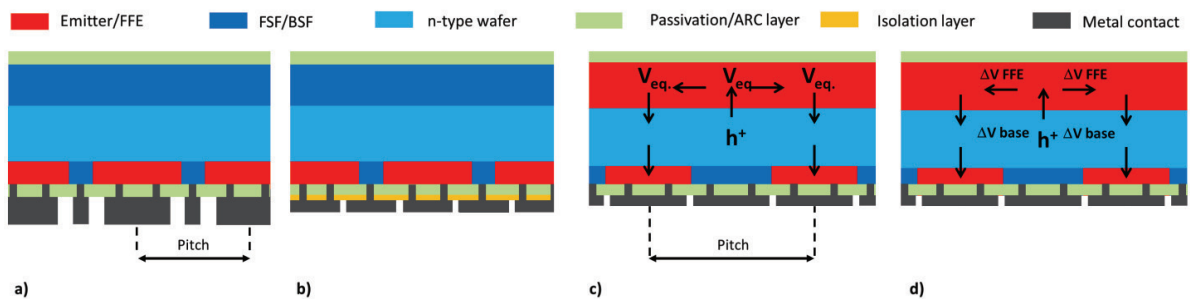


Fig. 1. Design variation of conventional IBC cell with interdigitated polarity structure on the rear and Front Surface Field (FSF); a) with emitter metal redundancy, and b) with insulating layer. c) Novel design variation on an n-type IBC cell, which we name Mercury cell, featuring a relatively conductive front floating emitter and a rear with equal contact cross-sections and a larger cell pitch due to a wide BSF. The arrows depict the flow path that holes take to the rear emitter when generated above the BSF area. d) The Mercury cell with relatively high resistive FFE and wafer resulting in a potential drop in both parts of the cell.  $V_{eq}$  is the equipotential of the FFE.  $\Delta V$  shows a lateral potential variation (in FFE or in base). The schematics a-d) are to illustrate the components of the cells and are not drawn to scale.

In this study we propose and report on a novel design variation of the traditional IBC cell, meant to enhance lateral transport properties for minority carriers. Owing to the enhanced transport distance, it simply allows the BSF width to be as wide as the emitter width without significant loss in cell efficiency. This enhancement is brought about by implementing a  $p^{++}$ -doped layer on the front of the n-type IBC cell, also referred to as front floating emitter (FFE), which induces a pumping effect on the holes from the BSF to the rear emitter as illustrated in Figure 1c and which is discussed in more detail in section 2. Although front floating emitters have been investigated in the past [9-17], the novelty presented in this paper resides in the proper tuning of the conductivity of the FFE and the wafer in combination with cell structure dimensions. With proper tuning, the FFE can be applied as an effective means to increase the BSF width with marginal loss in cell performance while assuring process simplification and cost reduction. Besides this, the new design leads to more freedom in the interconnection lay-out and increases the tolerances for the module fabrication. We name this invention the Mercury cell, in reference to the planets' proximity to the sun. Moreover we present both 2D numerical simulation results and experimental evidence for the working principle.

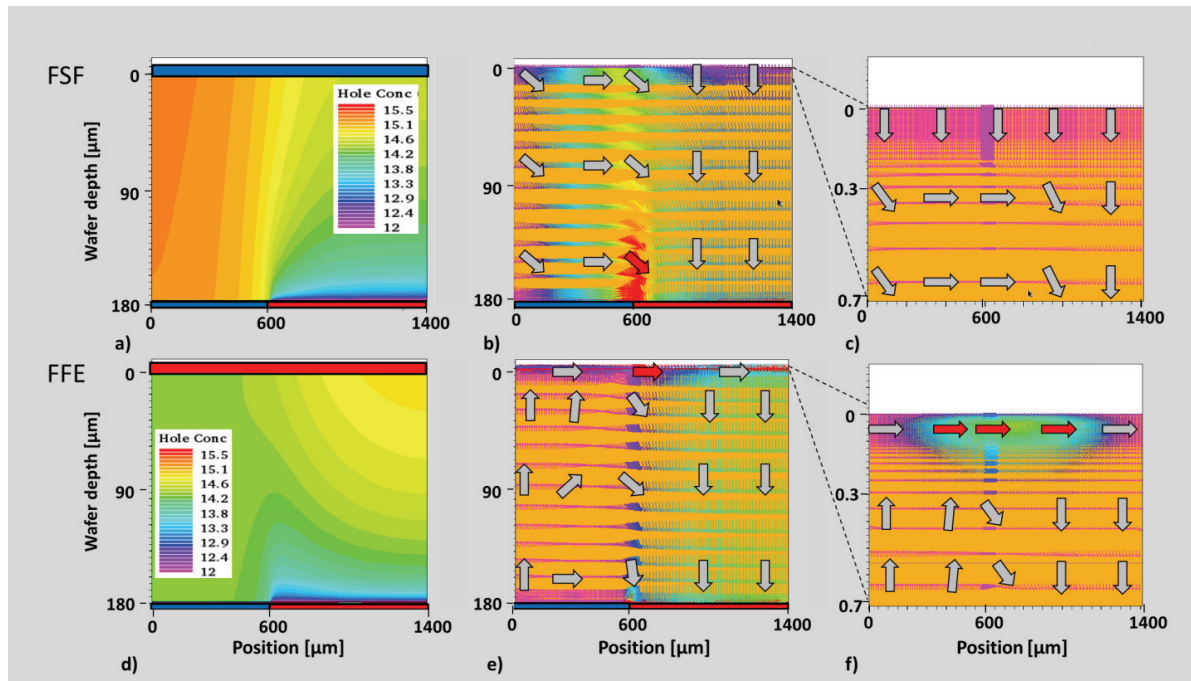


Fig. 2. Simulated (Atlas) performance comparison of the n-IBC cell with FSF or FFE on n-type wafer at  $J_{sc}$  condition. a & d) Illustration of the hole carrier density [ $h^+$ ] of an extremely wide BSF of 1200  $\mu\text{m}$  (full width). [ $h^+$ ] in  $\text{cm}^{-3}$ , contours coloured as  $\log_{10}([h^+])$ . Images b, c, e, f are vector plots illustrating the size and direction of the holes current for a FSF cell (b, c) and FFE cell (e, f). Images c and f are zoomed in at the surface diffusion of FSF and FFE respectively. The y-axis' measures the distance from the top surface into the wafer in microns and the x-axis' measures the distance from the centre of the BSF (blue bar) to the centre of the emitter (red bar). The red arrows in the vector plots indicate high current densities.

## 2. Working principle of Mercury cell

The working principle of an IBC cell with a front floating emitter has been explained in previous work in terms of equivalent circuits that prominently incorporated a transistor element to describe the p/n/p bipolar transistor action above the rear emitter [15-16]. Here we focus on the relation between electrical shading and cell design parameters such as the resistance of the FFE and the wafer and BSF width.

Under illumination, a front floating emitter collects minorities from the base as schematically illustrated in Figure 1c. In principle, since the FFE is not contacted, these carriers are not extracted and the FFE-base junction will be charged towards open circuit condition. If the FFE is conductive enough, the FFE will be a near equipotential surface,  $V_{eq}$ , over the full surface of the wafer. The working principle of the Mercury cell is an asymmetry in the working point of the I-V curves of the FFE-base junction. Above the BSF, the junction where most carriers will be collected, is the FFE. Above the emitter, both the FFE and the rear emitter can collect carriers. Hence, the photocurrent across the FFE-base junction is smaller above the rear emitter than above the BSF. This means that when the FFE-base junction above the BSF is in open circuit, and because of the laterally constant potential in the FFE, the FFE-base junction above the emitter is operating below open circuit voltage. This sets up a hole transport “conveyor belt”: minorities (holes) generated above the BSF are collected in the FFE and transported as majorities towards regions above the rear emitter, where they are re-injected into the base and subsequently collected by the rear emitter. Effectively, the front junction collects the minority carriers from the base and transports them to the section where the front emitter overlaps with the emitter on the rear, as is illustrated in Figure 2.

This current flow from FFE to emitter will be in addition to the diffusion of minority carriers directly from the base to the rear emitter junction. In addition to providing enhanced lateral transport, the pumping effect drastically reduces carrier levels in the base, and hence the recombination rate in the base. This reduced carrier concentration is illustrated in Figure 2 a and d, where the case of a FSF cell shows much higher minority carrier densities than the case of an FFE cell.

The re-injection of carriers from the FFE above the emitter into the base does however lead to a higher  $[h^+]$  concentration near the front surface above the rear emitter junction in the FFE case than the FSF case, as can be seen in Figure 2 a and d. However, much smaller  $[h^+]$  concentration gradients are required for vertical minority carrier transport from front to rear than from left to right from above BSF to rear emitter. This is explained by the geometry of the system. For the vertical  $[h^+]$  transport in the FFE case, the full emitter width is available, whereas for the lateral  $[h^+]$  transport in the FSF case only the wafer thickness is available. So the same concentration gradient can transport more carriers in the FFE case. For the vertical transport in the FFE, the carriers need to cross only the wafer thickness, in the FSF case the carriers need to cross the BSF width leading to lower carrier concentrations, and hence less recombination. Combined, this leads to overall lower carrier concentrations, and hence less recombination.

The pumping effect of the FFE cell hence allows to increase the pitch of the cell, while maintaining a good current.

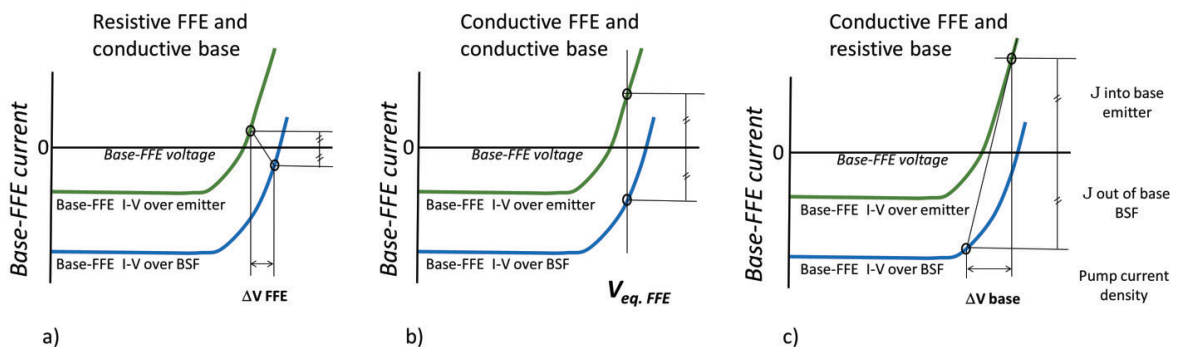


Fig. 3. The qualitative illustration on the mechanism of the pumping effect in the FFE showing the IV-curves of base-FFE junction above BSF and emitter for 3 cases of resistivity of FFE and wafer in order of increase pump current. The magnitude of the pump current  $I$  and the relevant voltage drop affecting it is illustrated in each case.

The pumping effect can be described qualitatively by the IV curves illustrated in the Figure 3. Here three cases a, b, and c are illustrated ranked in order of increasing pumping current. The first case (a) represents an IBC cell with a

relatively high resistive FFE and a relatively high conductive base, resulting in a low pumping current because the potential drop in the FFE moves the FFE-base junctions above the BSF and rear emitter to open circuit and charges only move in perpendicular direction with respect to the wafer surface. The second case (b) represents a cell with a relatively high conductive base as well as a relatively high conductive FFE. Here the pump current increases because the lateral potential drop in the FFE and base is near zero and both regions of the FFE-base junctions are at equal operating voltage. The largest pump current is obtained in case (c) with a relatively high conductive FFE and relatively high resistive base. Here, the lateral potential variation in the n-type base, caused by lateral flow of electrons from the bulk above the rear emitter to the BSF contact, represents an extra driving force for the pump effect. It moves the operating voltages closer to the current collecting plateau of the IV curve for the BSF region and drives the emitter region of the FFE-base junction to further forward bias. If on the other hand the resistance in the FFE increases, the driving force for the pump current is countered. From the consideration above it becomes clear that a relatively high resistive wafer and a relatively high conductive FFE are desired for hole transport in an IBC cell with FFE and a broad BSF width. In other words, the distance over which the holes can be transported above the BSF increases with the conductivity of the FFE and the resistance of the wafer, allowing to increase the BSF width of the cell, while maintaining a good minority carrier collection at the rear emitter.

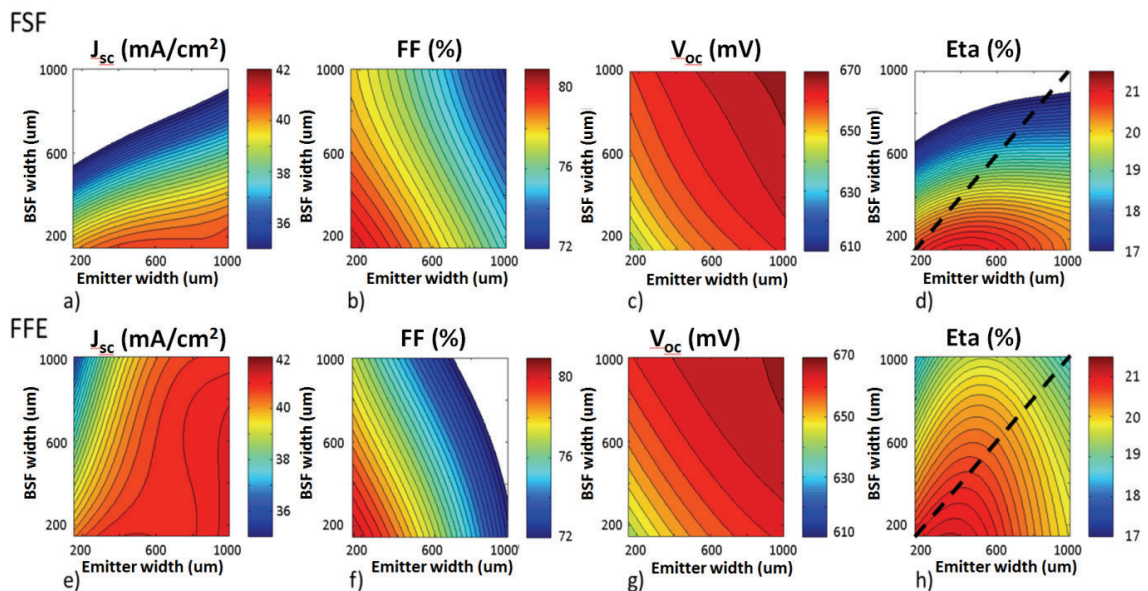


Fig. 4. Modelled performance comparison of the IBC cell with FSF and FFE. The IV parameters  $J_{sc}$ , FF,  $V_{oc}$  and cell efficiency are presented as a function of emitter and BSF width. The values shown are based on the unit cell and are thus half-widths and are expressed in  $\mu\text{m}$ . The diagonal dashed line in d) and h) indicates cell designs with equal widths for emitter and BSF.

It can be argued that the FFE does not enhance the lateral transport of majorities in the base as an IBC cell with a FSF is expected to do, as suggested by Granek et al. [18]. As a result thereof, it would lower the FF of the Mercury cell relatively to the FSF cell. It is good to mention here, however, that this hypothesis is challenged in a recent publication of Ohrdes et al. [19]. Here, the benefit of a FSF is discussed compared to a undiffused and passivated surface. It was found that FF improvements due to a FSF are caused by changes in surface recombination instead of to reduction in ohmic losses. Even so, it can be appreciated that the IBC cell with a relatively conductive FFE allows to increase the BSF width compared to the FSF cell, without the stringent penalty of electrical shading losses. Consequently, the BSF fraction in the cell increases and as a result thereof a larger fraction of the majority carriers is generated above the BSF which reduces the ohmic losses associated with lateral transport of majorities in the cell. Obviously, due to a wider BSF region, the ohmic losses of holes in the FFE increase as the distance the holes need to

travel in the FFE to the rear emitter region increases. Therefore, the possible gain in FF due to lower ohmic losses of electrons in the base (low emitter fraction) is reduced.

### 3. Simulation results

Based on 2D simulations conducted with Quokka, we demonstrate in Figure 3, that the lateral effective transport length can be increased and that the electrical shading losses and the cell efficiency are less dependent on the BSF width in the Mercury concept than in the conventional IBC cell with FSF. Furthermore, this design tolerance can be achieved at similar cell efficiencies. The presented data are calculated for IBC cells with screen-printed single contacts per polarity, which generally lower the  $V_{oc}$  of the cells due to significant contact recombination. The input parameters for  $J_o$ ,  $R_{sheet}$  and  $t_{bulk}$  are tabulated in the appendix. The most striking difference between both cells is the  $J_{sc}$  behaviour for changing width of emitter and BSF. Whereas the  $J_{sc}$  plummets for the FSF cell with broad BSF widths due to electrical shading losses, the FFE cell maintains high currents for a large part of the parameter space. The fill factor of the FFE cell is slightly lower than of the FSF cell while the  $V_{oc}$  is identical as the  $J_o$  values are kept similar for both cells. The FF presented in Figure 4, includes practical ohmic losses in the contacts, finger and busbars. The resulting efficiency plots clearly show that high cell efficiencies can be obtained for a broad range of cell geometries including the case of equal widths and reasonable cell pitch which are preferred with respect to the optimal metallization solutions as discussed earlier.

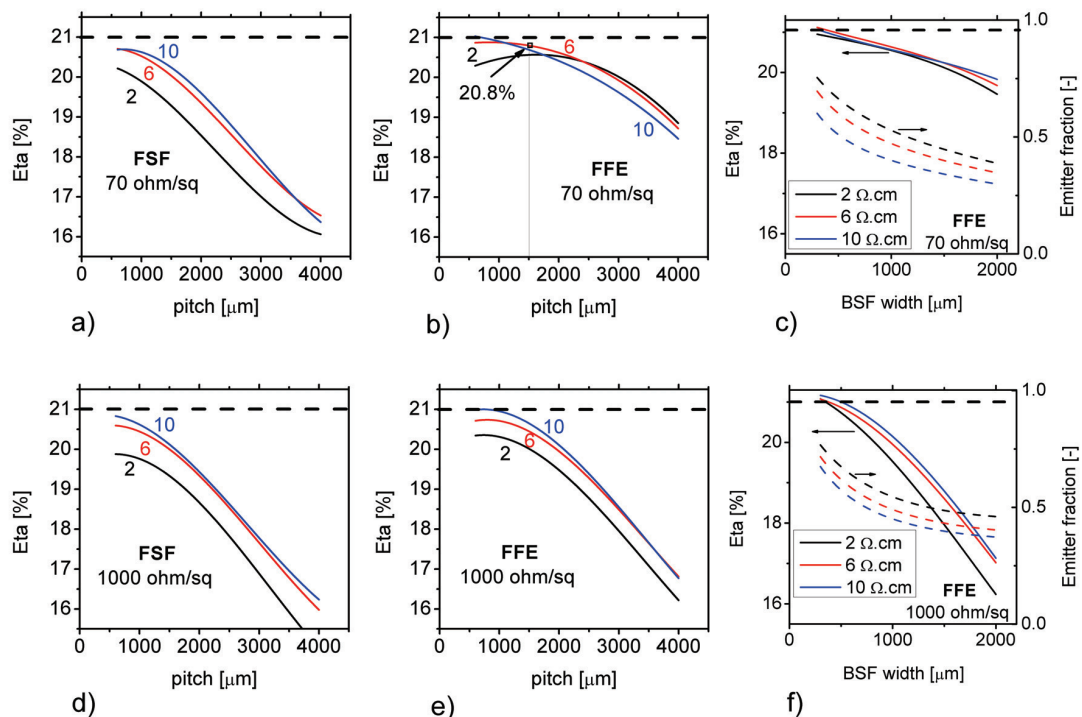


Fig. 5. Modeled conversion efficiency vs. pitch comparison of FSF and FFE IBC cell with equal emitter and BSF widths (a,b,d,e). The performance is evaluated for relatively conductive (70  $\Omega$ /sq) and relatively resistive (1000  $\Omega$ /sq) front diffusions and 2, 6 and 10  $\Omega$ .cm wafers at a bulk lifetime of 2 ms. In c, f the path of least efficiency decay is shown for BSF widths between 0 and 2 mm (full width) and its corresponding emitter fraction. The optimal efficiency of the 70  $\Omega$ /sq FSF cell on a 6 to 10 ohm.cm wafer with narrow BSF (340  $\mu$ m) and emitter (840  $\mu$ m) is marked by the dashed line in all graphs.

#### 4. Mercury cell design

To illustrate the potential of the Mercury cell design, an IBC cell with conductive FFE and broad BSF, we evaluate in Figure 5 the conversion efficiency dependency on the cell pitch for IBC cells with equal widths for emitter and BSF with screen printed fingers. This is done for IBC cells with varying sheet resistance of the front diffusion and different wafer resistivities. From the Figure 5b, it becomes apparent that the efficiency of the Mercury cell with a 70 Ω/sq FFE and a 6 Ω.cm wafer, nearly saturates at 20.8%. This plateau is reached for cell pitches up to 1.5 mm which are cell dimensions that can be practically made. A further increase of the pitch up to 2.3 mm can be achieved at the expense of 0.3% lower efficiency. It should be noted that at lower bulk lifetimes the electrical shading losses in the FSF cell increase more strongly than for the FFE cell due to the lower carrier density in the Mercury cell as discussed above. Consequently, the benefits of the Mercury cell are more pronounced at lower bulk lifetimes than the 2 ms lifetime used in the illustrated simulation. For fair comparison to the conventional IBC cell, it is required to compare the efficiency of the Mercury plateau to that of the optimal FSF IBC cell with a narrow BSF. The optimal FSF cell efficiency at a BSF and emitter width of 340 and 840 μm respectively is 21.0% which is only marginally higher (0.2% absolute) than the Mercury plateau. Finally, the Mercury cell with relatively high resistive FFE approaches the pitch dependency of the FSF cell due to the deminished pumping current caused by the significant voltage drop that builds in the FFE as the pitch and thus the BSF width increases.

In Figure 4h we can see that for every BSF width there is an emitter width that gives optimum efficiency. We plot in Figure 5c and 5f, for completeness, as a function of BSF width the maximum efficiency attainable for that BSF width (solid colored lines), and the emitter width that corresponds to that maximum (expressed as fraction of the total pitch, dashed colored lines).

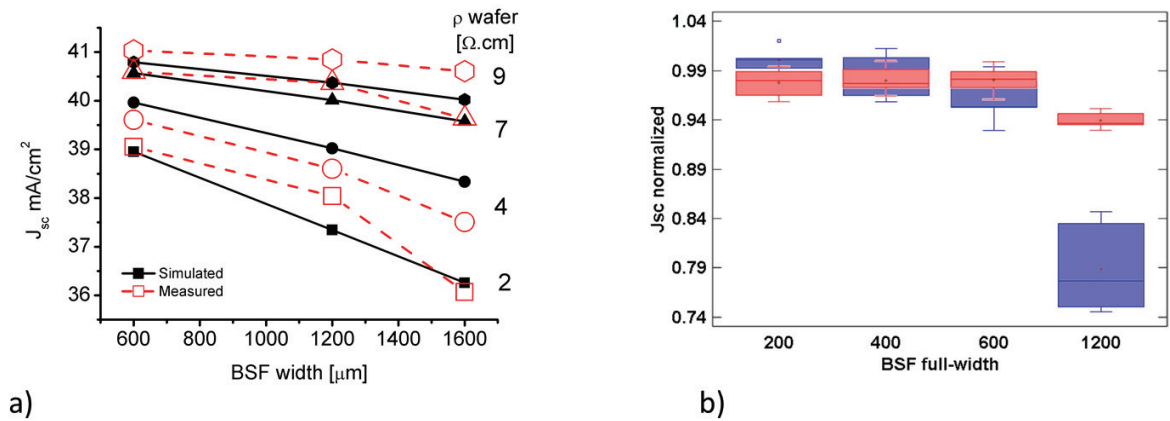


Fig. 6. a) Simulated and experimental values for  $J_{sc}$  of the Mercury cells with different wafer resistivity and different BSF full widths. The emitter width is fixed to 1600 μm. b) Normalized short-circuit densities,  $J_{sc}$ , as a function of BSF width measured on small-sized IBC cells (~13 cm<sup>2</sup>) with FSF (blue) and FFE (red).

#### 5. Validation

Wafers with different bulk resistivity were taken from a single ingot to study the effect of the wafer resistivity and BSF width on the I-V parameters of the Mercury cell. Resistivity values of 2, 4, 7 and 9 Ω.cm were chosen for investigation. Mercury cells featuring an emitter width of 1600 μm and three different BSF widths (600, 1200 and 1600 μm) were manufactured. The  $J_{sc}$  results are presented in Figure 6, and clear trends are observed. In all cases, the  $J_{sc}$  increases with higher wafer resistivity ( $\rho$ ). In addition, the slope of the  $J_{sc}$  as function of the BSF width decreases with  $\rho$ . Generally, for both IBC cells, but mostly for the FSF IBC cell,  $J_{sc}$  suffers from higher doping levels as this results in higher SRH recombination rates especially in the bulk due to increased carrier concentrations.

However, for the FFE cell also the pumping effect is enhanced by the higher wafer resistance as discussed in paragraph 2. The  $J_{sc}$  of the cells with high  $\rho$  wafers is nearly independent of the BSF width, which is in contrast to the large  $J_{sc}$  differences for BSF widths at low  $\rho$ .

These results were validated in ATLAS (Silvaco). For that purpose, a cross-section perpendicular to the fingers was simulated. The unit cell consisted of half a BSF and half an emitter. The physical models used were Klaassen's Unified Low-Field Mobility model, a Saturation Velocity Model according to Caughey and Thomas, Fermi-Dirac statistics, Klaassen's bandgap narrowing model, radiative recombination, temperature and concentration dependent Auger recombination and SRH recombination. Surfaces were treated as flat, however the increased recombination activity due to surface area increase by presence of a pyramidal texture was taken into account by multiplying Auger recombination coefficients near the surface with a factor of 1.7. Generation profiles were obtained from PC-1D for a case with texture on front- and rear side. Screen printed contacts were modelled by assuming that the firing process etches into the diffusion. Diffusion profiles were based upon ECV measurements of the actual doping profiles used in the experiment.

In an initial experiment, Mercury cells were compared to IBC cells with a front surface field (FSF). The  $J_{sc}$  decrease with increasing BSF width is especially pronounced for the cells with FSF, and much less for the cells with FFE, as shown in Figure 6b. It has to be noted that in this experiment the total pitch was fixed rather than the emitter width, so it is not possible to directly compare the results to the experiment with different wafer resistivities and BSF widths.

## 6. Implications for module design

So far, the discussion has focussed on the benefit of a conductive FFE at cell level to increase the BSF width with marginal loss in cell performance while increasing patterning tolerances assuring process simplification and cost reduction. Additional advantages of the conductive FFE are expected for the module interconnection especially to a conductive back-sheet such as used for MWT modules [20]. The ECN back-contact module interconnection technology is based on an interconnection foil with integrated conductor layer, on which the cells are electrically contacted using a conductive adhesive. Compared to a tab-based interconnection, the rear-side foil interconnection allows to reduce the module series resistance by using more interconnect metal (more cross-sectional area) and thereby reducing the cell-to-module FF loss.

Collected current needs to pass through broad busbars on the cell which can easily measure millimetres in width. In a FSF cell these areas would significantly increase electrical shading losses as calculated by Hermle et al. [8]. In this report an emitter and a BSF busbar of 3 mm on a 125 mm wafer would result in a 0.8% abs efficiency loss. This loss is nearly equally divided in FF loss above the emitter busbar and electrical shading losses above the BSF busbar. The Mercury cell would significantly mitigate the part of the electrical shading losses as illustrated in the previous sections. The flexibility of the conductive foil interconnection technology allows to increase the number of interconnection points while optimising their distribution on the cell. As a consequence, grid related series resistance can be reduced and busbars can be slimmed down allowing reduction of the metal load on the wafer.

## 7. Current experimental status

Mercury cells were processed on 156x156 mm<sup>2</sup> semi-square n-Cz wafers using the same process tools as our industrial n-pasha cell process. Screen printed metallization was used and an isolation gap between rear emitter and BSF is omitted. In parallel, substrates with multiple small cells were prepared to study the impact of the BSF width. On small cells, on which we only illuminated the active part of the cell between two emitter busbars but, including a BSF busbar, we obtained a maximum efficiency of 19.4% with a  $J_{sc}$  of 41.6 mA/cm<sup>2</sup> for a 600  $\mu$ m wide BSF. This is to our knowledge the highest  $J_{sc}$  value reported for n-type or p-type IBC solar cells employing a front floating emitter [9-17]. The high  $J_{sc}$  proves that bulk lifetime and front surface passivation are sufficient for near ideal current collection. Very high  $J_{sc}$  values up to 41.2 mA/cm<sup>2</sup> were even reached for cells with an extremely wide BSF of 1600  $\mu$ m, demonstrating the effectiveness of the Mercury concept. For the 6 inch cells we obtained a best cell efficiency of 19.0% as shown in Table 1. The efficiency loss of the Mercury cells at low bias light conditions compared to 1



sun was analysed. In contrast to earlier reports on linearity issues with IBC cells employing an FFE [9], the efficiency loss at low illumination intensity appeared to be less than for a standard p-type reference cell. The IV measurements have been conducted with a Class AAA solar simulator (Wacom).

By 2D modelling, we obtained insight in the main loss factors of the current cell design. Further improvement of passivation, diffusion profiles and interconnection design are likely to yield cell efficiencies between 21 and 22% on the short term using processing based on screen printed contacts. For PVD and/or plating type metallization we expect to achieve between 22-23% with the Mercury concept with the additional process and cost advantage of omitting the isolation steps due to equal widths in BSF and emitter diffusions.

Table 1. Current-Voltage parameters of best Mercury IBC cells (emitter width is 1600  $\mu\text{m}$ ).

Cell type	Active Area ( $\text{cm}^2$ )	$V_{oc}$ (mV)	$J_{sc}$ ( $\text{mA}/\text{cm}^2$ )	FF (%)	$\eta$ (%)
600 $\mu\text{m}$ BSF	13	627	<b>41.6</b>	74.2	19.4
1600 $\mu\text{m}$ BSF	13	629	<b>41.2</b>	73.1	18.9
1200 $\mu\text{m}$ BSF	<b>239</b>	635	40.5	73.9	<b>19.0</b>

## 8. Conclusion

We proposed a novel design variation of a tradition IBC cell, named the Mercury cell, that features a relatively conductive front floating emitter ( $\sim 70$  ohm/sq) and a broad BSF. This configuration significantly alleviates the problem of electrical shading especially at higher wafer resistivity and allows to design efficient IBC cells with interdigitated BSF and emitter regions of equal widths. Apart from relaxed alignment tolerances for the patterning and metallization steps of the solar cell process, equal widths of both polarities allow to metalize the IBC cell with blanket metallization technologies such as PVD and plating without the need of an isolation layer. This is a significant process simplification and thus a potential for cost reduction. We explain a working mechanism of the cell and present data that validates the model. So far our best cell efficiencies obtained for this cell concept are 19% on 6 inch cells with a BSF width of 1.2 mm. On 13  $\text{cm}^2$ , we reached 19.4% with an exceptionally high  $J_{sc}$  value of  $41.6\text{mA}/\text{cm}^2$  for a front floating emitter cell with an BSF width of 0.6mm. This high current was nearly maintained at an extremely wide BSF of 1.6 mm, illustrating excellent front passivation for efficient current collection and minimal electrical shading losses.

## Appendix: Simulation input parameters section 3

Table 2. Input parameters for Quokka simulation:

Diffusion	$j_0$ fA/ $\text{cm}^2$	Rsht
BSF	70	40
BSF contact	1500	40
emitter	60	70
emitter contact	3000	70
FSF	60	70
FFE	60	70
$t_{\text{bulk}}$	2ms	

## References

- [1] Smith et al. “SunPower’s Maxeon Gen III solar cell: High Efficiency and Energy Yield”, Proc. 39th IEEE PVSC, Tampa, 2013
- [2] Fong et al. , “Optimisation of n+ diffusion and contact size of IBC solar cells”, 28th EU-PVSEC, Paris (2013)
- [3] B. O’Sullivan et al., “Process simplification for high efficiency, small area interdigitated back contact silicon solar cells”, 28th EU-PVSEC, Paris (2013)
- [4] Bosch SE, press release (2013).
- [5] C.B. Mo et al., Proc. 27nd EU-PVSEC, Frankfurt, Germany (2012).
- [6] A. Halm et al. “The Zebra Cell Concept - Large Area n-Type Interdigitated Back Contact Solar Cells and One-Cell Modules Fabricated Using Standard Industrial Processing Equipment”, 27nd EU-PVSEC, Frankfurt, Germany (2012).
- [7] Dong et al., “High-Efficiency Full Back Contacted Cells Using Industrial Processes” Proc. 39th IEEE PVSC, Tampa, 2013
- [8] M. Hermle et al., “Shading Effects in Back-Junction Back-Contacted Silicon Solar Cells”, Proc. 33rd IEEE Photovoltaic Specialists Conference, St. Diego, CA, 2008.
- [9] Granek et al, “Analysis of the current linearity at low illumination of high-efficiency back-junction back-contact silicon solar cells”, phys. stat. sol. (RRL) 2, No. 4, 151–153 (2008)
- [10] Dicker et al., “Analysis of one-sun monocrystalline rear-contacted silicon solar cells with efficiencies of 22.1%”, JAP vol 91 ,7, 2002
- [11] P. Basore et al, “All-aluminum Screen-printed IBC Cells: Design Concept”, 39<sup>th</sup> IEEE PVSC, Tampa, 2013.
- [12] Robbelijn et al., “Towards advanced back surface fields by boron implantation on p-type interdigitated back junction solar cells”, Proc. 5th W-PVSEC, 6-10 September 2010
- [13] Chan et al.,” Simplified interdigitated back contact solar cells”, Proc. SiliconPV: April 03-05, 2012, Leuven, Belgium, published in Energy Procedia 27 ( 2012 ) 543 – 548
- [14] Gutiérrez et al., “Industrial manufacturing process of silicon TWT solar cell”, Proc. 28th EU-PVSEC, Paris, France (2004)
- [15] Jimeno et al. , “Modelling the TWT structure”, Proc. EU-PVSEC Paris, France (2004).
- [16] Sah et al., US patent nr 4665277, 1987
- [17] Sidhu et al., “Interdigitated Back Contact Silicon Solar Cells with Laser Fired Contacts”, Proc. 39th IEEE PVSC, Tampa, 2013
- [18] Granek et al.,”Enhanced lateral current transport via the front N+ diffused layer of n-type high-efficiency back-junction back-contact silicon solar cells”, Prog. Photovolt: Res. Appl. V17,1 p47-56, (2009)
- [19] Ordhes et al.,“High fill-factors of back-junction solar cells without front surface field diffusion”, 27th EU-PVSEC, Frankfurt, Germany (2012)
- [20] M.W.P.E. Lamers et al., “17.9% back-contacted mc-Si cells resulting in module efficiency of 17.0% ”, Proc. 25th EU-PVSEC, 2010, p.1417.